Journal for ImmunoTherapy of Cancer

^{89}Zr-pembrolizumab biodistribution is influenced by PD-1-mediated uptake in lymphoid organs

Elly L van der Veen ,[1] Danique Giesen,[1] Linda Pot-de Jong,[1] Annelies Jorritsma-Smit,[2] Elisabeth G E De Vries,[1] Marjolijn N Lub-de Hooge [2,3]

To cite: van der Veen EL, Giesen D, Pot-de Jong L, *et al*. ^{89}Zr-pembrolizumab biodistribution is influenced by PD-1-mediated uptake in lymphoid organs. *Journal for ImmunoTherapy of Cancer* 2020;**8**:e000938. doi:10.1136/jitc-2020-000938

► Additional material is published online only. To view please visit the journal online (http://dx.doi.org/10.1136/jitc-2020-000938).

Accepted 11 August 2020

[1]Department of Medical Oncology, UMCG, Groningen, Groningen, Netherlands
[2]Department of Clinical Pharmacy and Pharmacology, UMCG, Groningen, Groningen, Netherlands
[3]Department of Nuclear Medicine and Molecular Imaging, UMCG, Groningen, Groningen, Netherlands

Correspondence to
Dr Marjolijn N Lub-de Hooge; m.n.de.hooge@umcg.nl

ABSTRACT

Background To better predict response to immune checkpoint therapy and toxicity in healthy tissues, insight in the in vivo behavior of immune checkpoint targeting monoclonal antibodies is essential. Therefore, we aimed to study in vivo pharmacokinetics and whole-body distribution of zirconium-89 (^{89}Zr) labeled programmed cell death protein-1 (PD-1) targeting pembrolizumab with positron-emission tomography (PET) in humanized mice.

Methods Humanized (huNOG) and non-humanized NOG mice were xenografted with human A375M melanoma cells. PET imaging was performed on day 7 post ^{89}Zr-pembrolizumab (10 µg, 2.5 MBq) administration, followed by ex vivo biodistribution studies. Other huNOG mice bearing A375M tumors received a co-injection of excess (90 µg) unlabeled pembrolizumab or ^{89}Zr-IgG$_4$ control (10 µg, 2.5 MBq). Tumor and spleen tissue were studied with autoradiography and immunohistochemically including PD-1.

Results PET imaging and biodistribution studies showed high ^{89}Zr-pembrolizumab uptake in tissues containing human immune cells, including spleen, lymph nodes and bone marrow. Tumor uptake of ^{89}Zr-pembrolizumab was lower than uptake in lymphoid tissues, but higher than uptake in other organs. High uptake in lymphoid tissues could be reduced by excess unlabeled pembrolizumab. Tracer activity in blood pool was increased by addition of unlabeled pembrolizumab, but tumor uptake was not affected. Autoradiography supported PET findings and immunohistochemical staining on spleen and lymph node tissue showed PD-1 positive cells, whereas tumor tissue was PD-1 negative.

Conclusion ^{89}Zr-pembrolizumab whole-body biodistribution showed high PD-1-mediated uptake in lymphoid tissues, such as spleen, lymph nodes and bone marrow, and modest tumor uptake. Our data may enable evaluation of ^{89}Zr-pembrolizumab whole-body distribution in patients.

BACKGROUND

Immune checkpoint inhibitors targeting the programmed cell death protein-1 (PD-1/programmed death ligand-1 (PD-L1) pathway are showing impressive antitumor effects. However, not all patients respond and serious immune-related toxicity has been reported.[1] This has raised interest in better understanding the behavior of these drugs in the human body. PD-L1 and PD-1 are expressed by a broad range of immune cells, including T-cells, B-cells, natural killer (NK) cells, monocytes and dendritic cells. PD-L1 can be highly expressed by tumor cells, whereas PD-1 expression is most prominent in T-cells and lower in other immune cells.[2] Biodistribution of PD-1 and PD-L1 targeting drugs will likely be influenced by the dynamic expression patterns of these targets.

Molecular imaging has proven to be an useful tool for studying drug biodistribution.[3 4] In table 1, we summarized preclinical imaging studies that investigated biodistribution of radiolabeled molecules targeting PD-1 and PD-L1.[5–28] Most studies that we reviewed focused on tracer distribution in the tumor and its microenvironment, without considering PD-1 and PD-L1 expression in healthy immune tissues. Studies that do report on tracer uptake in lymphoid tissues are scarce and results are often limited to the spleen. Furthermore, most tracers targeting human PD-1/PD-L1 are not cross-reactive with murine proteins and relevant mouse models reconstituted with (parts of) a human immune system are rarely used. A limited number of studies used NOD *scid* gamma (NSG) mice engrafted with human peripheral blood mononuclear cells (hNSG model).[23–25 27] The hNSG model has a high level of functional T-cells, however, it is also characterized by aberrant distribution of immune cells to murine immune tissues and other cell lineages remain underdeveloped.[29] Humanized mice that are engrafted with human CD34 + hematopoietic stem cells (HSCs) establish an immune-competent model with a broader set of developed human immune cells present and might therefore be a better surrogate for the human immune environment.

To gain more insight in the in vivo behavior of a human PD-1 targeting monoclonal

Table 1 Preclinical imaging studies targeting PD-L1 and PD-1, using radiolabeled monoclonalantibody or small proteins

Type of Imaging	Tracer	Origin and reactivity	Cross reactivity	Animal model	Tumor model	Tracer dose	Imaging / biodistribution time point	Tumor uptake	Uptake lymphoid tissue	Ref
Anti-PD-L1 - antibodies										
SPECT/CT	^{111}In-PD-L1.3.1 antibody	Murine anti-human	No	Balb/c nude mice 6 to 8 weeks old Immune deficient	Human breast cancer cell lines	1.5 µg (15.5 MBq) and 1.0 µg (10.0 MBq)	Imaging and ex vivo biodistribution at 24, 72 and 168 hours pi	32.8 (±6.8) %ID/g and 6.2 (±1.0) %ID/g at 168 hours pi for MDA-MB-231 and MCF-7 tumors respectively PD-L1 detection at different expression levels in SK-Br-3, SUM149 and BT474 tumors	No	(5)
SPECT	^{111}In-DTPA-PD-L1 antibody	Hamster anti-mouse	No	*neu*-N transgenic mice 8 to 12 weeks old Immune competent	NT2.5 (mouse mammary tumor)	7.4 MBq for imaging and 8.4 µg (0.93 MBq) for biodistribution	Imaging on 1, 24, and 72 days pi and ex vivo biodistribution at 1, 24, 72, and 144 hours pi	Tumor uptake of 21.1 (±11.2) %ID/g at 144 hours pi	Yes, spleen (63.5%±25.4 %ID/g) and thymus (16.8%±16.2 %ID/g) at 144 hours pi Spleen uptake was blocked by coinjection of unlabeled antibody	(6)
SPECT	^{111}In-PD-L1 antibody	Humanized anti-human	Cross-reactive with mouse	NSG mice 6 to 8 weeks old Immune deficient	Human cell lines	100 µg (14.8 MBq) for imaging and 8.5 µg (1.48 MBq) for biodistribution	Imaging and ex vivo biodistribution at 24, 48, 72, 96 and 120 hours pi	8.9 (±0.26) %ID/g at 72 hours pi for MDA-MB-231 tumors and 7.46 (±0.12) at 144 hours pi for H2444 tumors Detection of PD-L1 at different expression levels	Yes, spleen (23.5±8.2) at 48 hours pi Spleen uptake was blocked by co-injection of unlabeled antibody	(7)
PET	^{64}Cu-PD-L1 antibody	Humanized anti-human	Cross-reactive with mouse	NSG mice 6 to 8 weeks old Immune deficient	Human cell lines	16.7 MBq (40 µg) for imaging and 1.48 MBq (10 µg) for biodistribution	Imaging on 2, 24 and 48 hours pi and ex vivo biodistribution at 24 and 48 hours pi	40.6 (±6.9) %ID/g, 17.2 (±2.1) %ID/g and 9.4 (±2.3) %ID/g at 48 hours pi for PD-L1 positive CHO, MDA-MB-231 and SUM149 tumors respectively	High spleen uptake (~45 %ID/g) at 24 hours pi after blocking with unlabeled antibody	(8)
				Balb/c mice 4 to 6 weeks old Immune competent	4T1 (mouse mammary carcinoma)			17.0 (±4.3) %ID/g at 48 hours pi for 4T1 tumors	No high uptake observed in spleen (±12 %ID/g) and BAT	
SPECT	^{111}In-DTPA-PD-L1 antibody	Rat anti-mouse	No	C57BL/6 mice 6 to 8 weeks old Immune competent	B16F10 (murine melanoma)	15–16 MBq (60 µg) for imaging and 0.37 MBq (0.13 mg/kg)	Imaging on 1, 24 and 72 hours pi and biodistribution at 1, 24, 72 and 96 hours pi	6.6 (±3.1) %ID/g at 24 hours pi for B16F10 tumors	Yes, spleen (47%±9.5 %ID/g) at 24 hours pi and BAT Spleen uptake was blocked by coinjection of unlabeled antibody	(9)
PET	^{89}Zr-anti-PD-L1 antibody	Rat anti-mouse	No	C57BL/6 mice 6 to 8 weeks old Immune competent	MEER (murine tonsil epithelium) or B16F10 (murine melanoma)	3.7 MBq (50 µg)	Imaging and ex vivo biodistribution at 48 and 96 hours pi	Higher uptake in irradiated (20.1%±2.6 %ID/g) vs non-irradiated (11.1%±1.9 %ID/g) MEER tumors Higher uptake in irradiated (28.0%±4.9 %ID/g) vs non-irradiated (14.4%±1.4 %ID/g) B16F10 tumors	Yes, spleen (60% to 120%ID/g) and thymus (25% to 35%ID/g) Spleen uptake was blocked by pre-injection of unlabeled antibody	(10)
PET	^{89}Zr-C4 (recombinant IgG1 antibody)	Engineered anti-human	Cross-reactive mouse	Nu/nu mice 3 to 5 weeks old Immune deficient	H1975 and A549 (human NSCLC), PC3 (human prostatic small cell carcinoma)	11.1 MBq for imaging and 1.85 MBq for ex vivo biodistribution	Imaging and ex vivo biodistribution at 8, 24, 48, 72, 120 hours pi	~9 %ID/g~5 %ID/g and ~7 %ID/g at 48 hours pi for H1975, A459 and PC3 tumors respectively ~13% ID/g at 48 hours pi for B16F16 tumors ~5 %ID/g tumor uptake at 48 hours pi in PDX model Detection of pharmacological-induced changes in PD-L1 expression	Yes, spleen uptake of ~7 %ID/g and ~6 %ID/g at 48 hours pi in nu/nu and C57BL/6 mice respectively Increased uptake in the spleens of nu/nu mice treated with paclitaxel and spleens of C57BL/6 mice treated with doxorubicin	(11)
				C57BL/6 mice 3 to 5 weeks old Immune deficient	B16F10 (mouse melanoma)					
				Not reported	PDX model of EGFR mutant (L858R) NSCLC					

Continued

Table 1 Continued

Type of Imaging	Tracer	Origin and reactivity	Cross reactivity	Animal model	Tumor model	Tracer dose	Imaging / biodistribution time point	Tumor uptake	Uptake lymphoid tissue	Ref
SPECT/CT	^{111}In-anti-mPD-L1	Rat anti-murine	No	Balb/c and C57BL/6 6 to 8 weeks old Immune competent	Murine cell lines	19.7 (±1.2) MBq (30 µg)	Imaging and ex vivo biodistribution at 72 hours pi	~14.53 (±5.49) %ID/g,~16.29 (±5.57) %ID/g,~11.06 (±6.54) %ID/g,~14.94 (±4.01) %ID/g,~6.16 (±2.94) %ID/g, for Renca, 4T1, CT26, B16F1 and LLC1 respectively	Yes, spleen varying from 13.09 %ID/g to 40.30 %ID/g. Thymus varying from 6.09 %ID/g to 10.26 %ID/g	(12)
	^{111}In-anti-hPD-L1	Murine anti-human	No	Non-humanized and humanized NSG mice	MDA-MB-231 (human breast carcinoma)	11.9±1.6 MBq (1 µg) ^{111}In-anti-hPD-L1 Or 11.5±0.4 MBq (2.8 µg) ^{111}In-control mIgG1 LPS treatment 1 day before tracer injection	Imaging and ex vivo biodistribution at 72 hours pi	~40 %ID/g for non-humanized mice and ~60 %ID/g for humanized mice at 72 hours pi ~35 %ID/g for humanized mice after LPS treatment at 72 hours pi ~8 %ID/g for ^{111}In-control mIgG1 in both non-humanized and humanized mice at 72 hours pi	Yes, spleen uptake ~20% ID/g for non-humanize mice and ~25% ID/g for humanized mice ~80 %ID/g for humanized mice after LPS treatment at 72 hours pi ~10 %ID/g for ^{111}In-control mIgG1 (both groups	
	^{111}In-anti-mPD-L1	Rat anti-murine	No	Balb/c and C57BL/6 6 to 8 weeks old Immune competent	Murine cell lines	Irradiation followed on day one by injection of 23.8±1.7 MBq (30 µg)	Imaging and ex vivo biodistribution at 24 hours pi	Higher uptake in irradiated (26.3%±2.0 %ID/g) vs non-irradiated (17.1%±3.1 %ID/g) CT26 tumors Higher uptake in irradiated (15.7%±1.8 %ID/g) vs non-irradiated (12.3%±1.7% ID/g) LLC1 tumors No difference uptake in irradiated (14.9%±6.8 %ID/g) vs non-irradiated (16.7%±3.5% ID/g) for B16F1 tumors	Spleen uptake ~14% to 17%ID/g for all models Higher uptake in lymph nodes of irradiated tumor models vs non-irradiated tumor models	
Anti-PD-L1 - small molecules										
PET	^{64}Cu-WL12 (PD-L1 binding peptide)	Engineered anti-human	No	NSG mice 6 to 8 weeks old Immune deficient	High PD-L1-expressing CHO cell line	5.6 MBq for imaging and 1.5 MBq for ex vivo biodistribution	Imaging and ex vivo biodistribution at 10 min, 0.5, 1 and 2 hour pi	14.9 (±0.8) at 1 hour pi in hPD-L1-expressing CHO tumors	No	(13)
PET	^{18}F-AlF-NOTA-Z_{PD-L1} (anti PD-L1 small molecule, affibody)	Engineered anti-human affibody	No	SCID beige mice 6 to 8 weeks old Immune deficient	LOX-IMVI (human melanoma) and SUDHL6 (human B-cell lymphoma)	0.2 to 0.6 MBq	Dynamic PET scan during 90 min	2.56 (±0.33) %ID/g at 90 min pi for LOX tumors	No	(14)
SPECT	^{99m}TC-anti-PD-L1 nanobodies	Engineered anti-mouse nanobodies	Cross-reactive human	C57BL/6 mice (WT) vs CD8 depleted PD-L1 KO mice 6 weeks old Immune competent	TC-1 (mouse lung epithelial), WT TC-1 PD-L1+ vs CRISPR/Cas9-modified TC-1 PD-L1 KO	45 to 155 MBq (10 µg) nanobody	Imaging 1 hour pi and ex vivo biodistribution 80 min pi	1.7 (±0.1) %ID/g for WT and 1.1 (±0.3) %ID/g for KO at 80 min pi	Yes, spleen 11.4 (±1.4) %ID/g for WT and 1.6±0.2% ID/g for KO at 80 min pi Lymph node uptake 3.5 (±0.8) %ID/g for WT and 0.4 (±0.1) %ID/g for KO at 80 min pi	(15)
PET	^{64}Cu-PD-1 ectodomain targeting PD-L1	Engineered anti-human	Not specified	NSG mice Immune deficient	CT26 (mouse colon cancer) hPD-L1 (+) or hPD-L1(-)	8.5 MB (25 µg)	Imaging at 1, 2, 4, and 24 hours. Ex vivo biodistribution at 1 and 24 hours	~3 %ID/g for PD-L1 (+) and ~1.8 %ID/g for PD-L1 (-) at 24 hours pi	Yes, spleen ~5 %ID/g at 24 hours pi	(16)

Continued

Table 1 Continued

Type of Imaging	Tracer	Origin and reactivity	Cross reactivity	Animal model	Tumor model	Tracer dose	Imaging / biodistribution time point	Tumor uptake	Uptake lymphoid tissue	Ref
PET	^{18}F-BMS-986192 (anti-PD-L1 small molecule)	Engineered anti-human	Affinity for human & cynomolgus PD-L1, no binding to murine PD-L1)	Immune deficient mice	Human L2987 (PD-L1+) and HT-29 (PD-L1-)	5.6 MBq, block to 3 mg/kg	Dynamic PET scan during 120 min	2.41 (±0.29) %ID/g for PD-L1 +and 0.82 (±0.11) %ID/g for PD-L1-, 0.79 (±0.12) %ID/g after blocking in PD-L+	Yes, spleen uptake (no clear numbers)	(17)
				Cynomolgus monkeys	–	55.5 MBq	Dynamic PET scan during 150 min	–	Yes, spleen:muscle 12:1, after blocking spleen:muscle1.24:1	
PET	^{64}Cu-PD-1 ectodomains (DOTA-/NOTA-HAC, aglycosylated DOTA-/NOTA-HACA)	Engineered anti-human	Not specified	NSG mice 6 to 8 weeks old Immune deficient	CT26 (mouse colon cancer) hPD-L1(+) or hPD-L1(-)	0.7–3.7 MBq (10 to 15 µg)	Imaging and ex vivo biodistribution at 1 hour pi	1.8 (±0.2) %ID/g for PD-L1(+) and 0.9 (±0.7) %ID/g PD-L1(-) for ^{64}Cu-NOTA-HAC-PD1 at 1 hour pi 4.2 (±0.8) %ID/g for PD-L1(+) and 3.5 (±1.7) %ID/g for PD-L1(-) for ^{64}Cu-NOTA-HAC-PD1 at 1 hour pi 2.7 (±1.1) %ID/g for PD-L1(+) and 0.8 (±0.4) %ID/g for PD-L1(-) for ^{64}Cu-NOTA-HACA-PD1 at 1 hour pi	Yes, spleen 4.0 (±3.1) %ID/g, 5.5 (±1.4) %ID/g and 1.4 (±0.4) %ID/g for ^{64}Cu-DOTA-HAC-PD1, ^{64}Cu-NOTA-HAC-PD1, and ^{64}Cu-NOTA-HACA-PD1 respectively	(18)
	^{68}Ga- PD-1 ectodomains (DOTA-/NOTA-HAC, aglycosylated DOTA-/NOTA-HACA)	Engineered anti-human	Not specified	NSG mice 6 to 8 weeks old Immune deficient	CT26 (mouse colon cancer) hPD-L1(+) or hPD-L1(-)	0.7 to 3.7 MBq (10 to 15 µg)	Imaging and ex vivo biodistribution at 1 hour pi	3.8 (±1.6) %ID/g for PD-L1(+) and 1.7 (±1.3) %ID/g for PD-L1(-) for ^{68}Ga-NOTA-HACA-PD1 at 1 hour pi 2.8 (±1.5) %ID/g for PD-L1(+) and 0.8 (±0.1) %ID/g for PD-L1(-) for ^{68}Ga-DOTA-HACA-PD1 at 1 hour pi	Yes, spleen 3.5 (±0.6) %ID/g and 0.2 (±0.2) %ID/g for ^{68}Ga-NOTA-HACA-PD1 and ^{68}Ga-DOTA-HACA-PD1 respectively	
PET	^{64}Cu-FN3$_{hPD-L1}$	Small molecule anti-human	No		CT26/hPD-L1	3.7 (±0.4) MBq (8 to 10 µg)	Imaging at 0.5, 1, 4, 18, and 24 hours pi followed by ex vivo biodistribution	5.6 (±0.9) %ID/g at 24 hours pi for CT26/hPD-L1 tumors	No	(19)
					MDA-MB-231 (human breast cancer)			3.6 (±0.5) %ID/g at 24 hours pi for MDA-MB-231 tumors		
PET	^{68}Ga-WL12 (PD-L1 binding peptide)	Engineered anti-human	No	NSG mice 6 to 8 weeks old Immune deficient	Human cell lines	±7.4 MBq for imaging and ±0.9 MBq for ex vivo biodistribution	Imaging and ex vivo biodistribution at 15, 60, and 120 min pi	11.56 (±3.18) %ID/g, 4.97 (±0.8) %ID/g and 1.9 (±0.1) %ID/g for hPD-L1, MDA-MB-231 and SUM149 tumors respectively at 60 min pi	No	(20)
PET	^{64}Cu-WL12 (PD-L1 binding peptide)	Engineered anti-human	No	NSG mice 5 to 6 weeks old Immune deficient	Human cell lines: H226, HCC827, CHO-hPD-L1+, CHO-hPDL1-, MDAMB231	±7.4 MBq for imaging and ±0.74 MBq for ex vivo biodistribution	Imaging and ex vivo biodistribution at 120 min pi Treatment with atezolizumab 24 hours prior to tracer injection (20 mg/kg)	~5.5 %ID/g,~8 %ID/g,~18 %ID/g,~5 %ID/g,~8 %ID/g for H226, HCC827, CHO-PDL1+, CHO-PDL1- and MDAMB231 respectively at 120 min pi Treatment reduced uptake in all cell lines? Tumors models?	Yes, spleen ~4 %ID/g, after treatment ~3.5 %ID/g	(21)
Anti-PD1 - antibodies										
PET	^{64}Cu-PD-1 antibody	Hamster anti-mouse	No	Treg+transgenic mice (Foxp3+.LuciDTR) Immune competent	B16F10 (mouse melanoma)	7.4 (±0.4) MBq (10–12 µg) Blocking with fivefold molar excess	Imaging and ex vivo biodistribution at 1 hour, 24 hours, and 48 hours pi	7.4 (±0.71) %ID/g for non-block vs 4.51 (±0.26) %ID/g for blocking 48 hours pi	Yes, spleen 23.04 (±4.97) %ID/g for non-block vs 14.39±0.53) %ID/g for blocking 48 hours pi	(22)

Continued

Table 1 Continued

Type of Imaging	Tracer	Origin and reactivity	Cross reactivity	Animal model	Tumor model	Tracer dose	Imaging / biodistribution time point	Tumor uptake	Uptake lymphoid tissue	Ref
PET	^{89}Zr-pembrolizumab	Humanized anti-human	Not specified	NSG and humanized NSG mice (hNSG)	A375 (human melanoma)	3.2 (±0.4) MBq (15 to 16 µg)	Imaging at 1, 4, 18, 24, 48, 72, 96, 120 and 144 hours pi, ex vivo biodistribution at 144 hours pi	1.8 (±0.4) %ID/g for NSG and 3.2 (±0.7) %ID/g for hNSG at 144 hours pi	Yes, spleen ~19 %ID/g for NSG and ~28 %ID/g for hNSG at 144 hours pi	(23)
	^{64}Cu-pembrolizumab					7.4 (±0.4) MBq (20 to 25 µg)	Imaging at 1, 4, 18, 24 and 48 hours pi, ex vivo biodistribution at 48 hours pi	5.7 (±0.6) %ID/g for NSG, 9.4 (±2.5) %ID/g for hNSG and 5.9 (±2.1) %ID/g for hNSG block at 48 hours pi	Yes, spleen ~6.5 %ID/g for NSG,~10.5 for hNSG, and ~7% ID/g for hNSG block at 48 hours pi	
PET	^{89}Zr-pembrolizumab	Humanized anti-human	No	ICR (CD-1) mice and Hsd Sprague-Dawley rats, 5 weeks old Immune competent	No tumor model	Mice: 5 to 10 MBq (7 to 14 µg) Rats: 50 MBq (14 µg)	Imaging at 3, 6, 12, 24, 48, 72, and 168 hours pi, ex vivo biodistribution at 168 hours pi	No tumor model	Yes, spleen ~2.5 %ID/g for mice and ~1% ID/g for rats 168 hours pi	(24)
				NSG mice and humanized NSG mice engrafted with human PBMCs (hu-PBL-SCID), 5–8 weeks old	No tumor model; PBMC engraftment			No tumor model	Yes, spleen ~8 %ID/g for NSG and ~4.5 %ID/g for hu-PBL-SCID) at 168 hours pi	
PET	^{89}Zr-Df-nivolumab	Humanized anti-human	No	NSG mice and humanized NSG mice engrafted with human PBMCs (hu-PBL-SCID 3–5 weeks old	A549 (human lung cancer)	5 to 10 MBq (7 to 14 µg)	Imaging at 3, 6, 12, 24, 48, 72, and 168 hours pi, and ex vivo biodistribution at 168 hours pi.	3.88 (±0.38) %ID/g for NSG and 9.85 (±2.73) %ID/g for hu-PBL-SCID at 168 hours pi 2.85 (±0.39) %ID/g for hu-PBL IgG control at 168 hours pi	Yes, 7.48 (±0.47) %ID/g for NSG and 4.32 (±0.40) %ID/g for hu-PBL-SCID) at 168 hours pi 3.05 (±0.79) %ID/g for hu-PBL-SCID IgG control at 168 hours pi	(25)
PET	^{89}Zr-nivolumab	Humanized anti-human	Affinity for cynomolgus monkey	Healthy non-human primates	–	54.5 (±11.0) MBq (237 µg)	Imaging at 24 hours, 96 hours, 144 hours and 192 hours	–	Yes, spleen at 192 hours SUV=17.63 Blocking 1 mg/kg at 192 hours SUV=2.5, 3 mg/kg SUV=2.62	(26)
PET	^{64}Cu-pembrolizumab	Humanized anti-human	No	Humanized NSG mice	293T (human embryonic kidney cell line) expressing hPD-L1 A375 (human melanoma)	7.4 (±0.4) MBq (20 to 25 µg)	Dynamic PET scans on 1, 2, and 4 hour pi during 3 min, at 18 and 24 hours pi during 5 min, at 24 hours pi during 10 min and at and 48 hours pi during 15 min Ex vivo biodistribution at 1, 12, 24, and 48 hours pi	14.8 (±1.2) %ID/g for 293T tumors at 48 hours pi 0.44 (±0.01) %ID/g for A375 tumors at 48 hours pi	Yes, spleen (17.5%±1.6 %ID/g) at 48 hours pi	(27)
Anti-PDL1 + anti-PD1 antibodies										
PET	^{64}Cu-PD-1 and ^{64}Cu-PD-L1 antibody	Murine anti-mouse	No	C57BL/6N mice PD-1-deficient mice PD-L1-deficient mice Immune competent	B16F10 (mouse melanoma)	1.13 (±0.31) MBq (1.5 µg) ^{64}Cu-PD-1 and 6.38 (±0.35) MBq (20 µg) ^{64}Cu-PD-L1	Dynamic PET scan during 45–55 and 15–20 min at 24 hours pi for ^{64}Cu-PD-1 and ^{64}Cu-PD-L1 respectively Ex vivo biodistribution at 48 hours pi	±14 %IA/cm^3 in B16F10 tumor at 24 hours pi in vivo for ^{64}Cu-anti-PD-1 and ^{64}Cu-anti-PD-L1 ±12 %IA/cm^3 in B16F10 tumor at 24 hours pi ex vivo for ^{64}Cu-anti-PD-L1	Yes, spleen (±20 %IA/cm^3) and lymph nodes (20%–30%IA/cm^3) for ^{64}Cu-PD-1, spleen (15 %IA/cm^3), lymph nodes (7.5%–15%IA/cm^3) and BAT (±12 %IA/cm^3) for ^{64}Cu-PD-L1 Detection of PD-1 +TILs after immunoradiothera-py PD-L1 upregulation (mainly in lung) by IFN-γ treatment visualized	(28)

WT; wild-type; AlF, aluminum fluoride; BAT, brown adipose tissue; DOTA, 1,4,7,10-tetraazacyclododecane- N,N',N'',N'''-tetraacetic acid ; DTPA, diethylenetriaminepentaacetic acid; EGFR, epidermal growth factor receptor; %ID/g, percentage of injected dose per gram; IFN-γ, interferon-gamma; KO, knock-out; LPS, lipopolysaccharide; NOTA, 1,4,7-triazacyclononane-N,N',N''-triacetic acid; NSCLC, non-small cell lung cancer; NSG, NOD SCID gamma; PBMC, peripheral blood mononuclear cell; PD-1, programmed cell death protein 1; PD-L1, programmed death-ligand 1; PDX, patient-derived xenograft; PET, positron emission tomography; pi, post-injection; SPECT, single photon emission CT; TILs, tumor-infiltrating lymphocytes.

antibody (mAb), not cross-reactive with murine PD-1, we aimed to study the biodistribution of zirconium-89 (^{89}Zr) radiolabeled pembrolizumab in melanoma-bearing humanized NOG mice (huNOG) engrafted with HSCs using positron-emission tomography (PET) imaging. To enable consecutive clinical translation of this approach, we developed and validated a good manufacturing practices (GMP) compliant production process for ^{89}Zr-pembrolizumab. Finally, we put our data in perspective by summarizing results from current in vivo preclinical studies with PD-1 and PD-L1 targeting radiolabeled molecules.

METHODS

Cell lines

The human melanoma cell line A375M was purchased from the American Type Culture Collection. Cell lines were confirmed to be negative for microbial contamination and were authenticated on August 6, 2018, by BaseClear using short tandem repeat profiling. A375M cells were routinely cultured in Roswell Park Memorial Institute 1640 medium (Invitrogen) containing 10% fetal calf serum (Bodinco BV), under humidified conditions at 37°C with 5% CO_2. Cells were passaged 1:10, twice a week. For in vivo experiments, cells in the exponential growth phase were used.

Development of ^{89}Zr-pembrolizumab and ^{89}Zr-IgG$_4$

First, the buffer of pembrolizumab (25 mg/mL, Merck) was exchanged for NaCl 0.9% (Braun) using a Vivaspin-2 concentrator (30 kDa) with a polyethersulfon filter (Sartorius). Next, pembrolizumab was conjugated with the tetrafluorphenol-N-succinyldesferal-Fe(III) ester (TFP-N-sucDf; ABX) as described earlier, in a 1:2 TFP-N-sucDf:mAb ratio.[30] Conjugated product was purified from unbound chelator using Vivaspin-2 concentrators and stored at −80 °C. On the day of tracer injection, N-sucDf-pembrolizumab was radiolabeled with ^{89}Zr, delivered as ^{89}Zr-oxalate dissolved in oxalic acid (PerkinElmer), as described previously.[30] For in vivo studies, pembrolizumab was radiolabeled at a specific activity of 250 MBq/mg. IgG$_4$ control molecule (Sigma-Aldrich) was conjugated with TFP-N-sucDf at a 1:3 molar ratio, followed by radiolabeling with ^{89}Zr at similar specific activity of 250 MBq/mg.

Quality control of ^{89}Zr-pembrolizumab

Size exclusion high-performance liquid chromatography (SE-HPLC) was used to determine the final number of TFP-N-sucDf ligands per antibody (chelation ratio). SE-HPLC analysis was also performed to assess potential aggregation and fragmentation for both N-sucDf-pembrolizumab and ^{89}Zr-pembrolizumab. An HPLC system (Waters) equipped with an isocratic pump (Waters), a dual wavelength absorbance detector (Waters), in-line radioactivity detector (Berthold) and a TSK-GEL G3000SWXL column (Tosoh Biosciences) was used with phosphate buffered saline (PBS, sodium chloride 140.0 mmol/L, sodium hydrogen phosphate 0.9 mmol/L, sodium dihydrogen phosphate 1.3 mmol/L; pH 7.4) as mobile phase (flow 0.7 mL/min). Radiochemical purity of ^{89}Zr-pembrolizumab was measured by trichloroacetic acid precipitation assay.[31] Immunoreactivity of ^{89}Zr-pembrolizumab was analyzed by a competition binding assay with unlabeled pembrolizumab. Nunc-immuno break apart 96-wells plates (Thermo Scientific) were coated overnight at 4°C with 100 µL of 1 µg/mL PD-1 extracellular domain (R&D Systems) in PBS, set to pH 9.6 with Na_2CO_3 2M. Plates were washed with 0.1% Tween 80 in PBS and blocked for 1 hour at room temperature (RT) with 150 µL 1% human serum albumin (Albuman, Sanquin) in PBS. Multiple 1:1 mixtures of ^{89}Zr-pembrolizumab with unlabeled pembrolizumab were prepared, using a fixed concentration of ^{89}Zr-pembrolizumab (7000 ng/mL) and varying concentrations of unlabeled pembrolizumab (from 3.75 ng/mL to 12.5×10^6 ng/mL). Of each mixture, 100 µL was added to the 96-wells plate and incubated for 2 hours at RT. After washing twice with washing buffer, radioactivity in each well was counted using a gamma counter (Wizard^2 2480–0019, SW 2.1, PerkinElmer). Counts were plotted against the concentration of competing unlabeled pembrolizumab. The half maximal inhibitory concentration (IC_{50}) was calculated using GraphPad Prism 7 (GraphPad software). Immunoreactivity was expressed as the IC_{50} value divided by the ^{89}Zr-pembrolizumab concentration to calculate the immune reactive fraction (IRF).

Animal studies

All animal studies were approved by the Institutional Animal Care and Use Committee of the University of Groningen. Studies were performed in humanized NOG mice (NOD.Cg-Prkdc^{scid} Il2rg^{tm1Sug}/JicTac, Taconic) and non-humanized NOG mice (Taconic) were used for control experiments. HuNOG mice are sublethally irradiated 3 weeks after birth and subsequently reconstituted with human CD34$^+$ hematopoietic stem cells derived from fetal cord blood to express a functional human immune system including B-cells, T-cells, NK-cells, dendritic cells and monocytes. HuNOG and NOG mice were subcutaneously xenografted with 5×10^6 A375M human melanoma cells in 300 µL of a 1:1 mixture of PBS and Matrigel (BD Biosciences) on the right flank. Tumor growth was assessed by caliper measurements. When tumor volumes reached 100 to 200 mm^3 (after 2 weeks), 2.5 MBq ^{89}Zr-pembrolizumab (10 µg) was administered via retro-orbital injection. Mice were anesthetized using isoflurane/medical air inhalation (5% induction, 2.5% maintenance).

The first group of huNOG mice received 10 µg ^{89}Zr-pembrolizumab (n=5). In addition, a second group of huNOG mice xenografted with the same tumor model received a co-injection of 10 µg ^{89}Zr-pembrolizumab and 90 µg unlabeled pembrolizumab (n=4). To a third group of huNOG mice, 2.5 MBq ^{89}Zr-IgG$_4$ control (10 µg) was administered (n=4). Control NOG mice received 10 µg ^{89}Zr-pembrolizumab (n=4).

PET imaging and ex vivo biodistribution

On day 7 post tracer injection (pi), PET scanning was performed. We selected this day based on optimal tumor-to-blood ratio and technical aspects, including feasible tracer specific activity and animal welfare. Mice were placed in a Focus 220 rodent scanner (CTI Siemens) on heating matrasses. Acquisition time was 60 min. A transmission scan of 515 s was performed using a ^{57}Co point source to correct for tissue attenuation. After scanning, mice were sacrificed for ex vivo biodistribution. Bone marrow was collected from the femur bone by centrifugal-based separation. All other organs were dissected and counted in a gamma-counter (Wizard^2 2480–0019, SW 2.1, PerkinElmer). Tracer uptake in each organ was expressed as percentage of the injected dose per gram tissue weight, calculated by the following formula: %ID/g = (activity in tissue (MBq)/total injected activity (MBq))/tissue weight (g)×100. To compare ex vivo and in vivo uptake, ex vivo uptake was also calculated as mean radioactivity per gram tissue, adjusted for total body weight ($SUV_{mean\ ex\ vivo}$), calculated with the following formula: $SUV_{mean\ ex\ vivo}$ = (activity in tissue (MBq)/total injected activity (MBq))×mouse weight (g). Calculations are corrected for decay and background.

PET data was reconstructed and in vivo quantification was performed using PMOD software (V.4.0, PMOD technologies LCC). Three-dimensional regions of interest were drawn around the tumor. For other organs and tissues, a size-fixed sphere was drawn in representative tissue parts. PET data was presented as mean standardized uptake value ($SUV_{mean\ in\ vivo}$), calculated by the following formula: SUV_{mean} (g/mL) = (activity concentration (Bq/mL)/applied dose (Bq))×weight (kg)×1000.

Autoradiography

Tumor and spleen from ex vivo biodistribution studies were formalin-fixed and paraffin embedded (FFPE). FFPE tissue blocks where cut into slices of 4 µM. These slices were exposed to a phosphor imaging screen (PerkinElmer) for 72 hours and then scanned using a Cyclone phosphor imager (PerkinElmer).

Immunohistochemistry

Subsequent slices of the same tumor, spleen and mesenteric lymph node tissue were stained for H&E, CD3, CD8 and PD-1. FFPE tumor, spleen and lymph node tissue were cut into 4 µm slices using a microtome (Microm Hm 355 s, Thermo Scientific) and mounted on glass slides. Tissue sections were deparaffinized and rehydrated using xylene and ethanol. Heat-induced antigen retrieval was performed in citrate buffer (pH=6) at 100°C for 15 min. Endogenous peroxidase was blocked by 30 min incubation with 0.3% H_2O_2 in PBS. For CD3 staining, slides were incubated with rabbit anti-human CD3-antibody (Spring bioscience; clone SP162) in a 1:100 dilution in PBS/1% bovine serum albumin (BSA) at RT for 15 min. For CD8 staining, slides were incubated with rabbit anti-human CD8-antibody (Abcam; clone SP16) in a 1:50 dilution in PBS/1% BSA at 4°C overnight. For PD-1 staining, slides were incubated with rabbit anti-human PD-1-antibody (Abcam, clone EPR4877(2)) in a 1:500 dilution in PBS/1% BSA at RT for 30 min. Human tonsil or lymph nodes tissues sections served ad positive control and were incubated with either CD3, CD8 or PD-1 antibody. As a negative control human tonsil or lymph nodes sections were incubated with rabbit IgG monoclonal antibody (Abcam, clone EPR25A) or PBS/1% BSA.

For CD3, CD8 and PD-1 staining, incubation with secondary antibody (anti-rabbit EnVision$^+$, Dako) was performed for 30 min, followed by application of diaminobenzidine chromogen for 10 min. Hematoxylin counterstaining was applied and tissue sections were dehydrated using ethanol and imbedded using mounting medium (Eukitt). H&E staining served to analyze tissue viability and morphology. Digital scans were acquired by a Nanozoomer 2.0-HT multi slide scanner (Hamamatsu).

^{89}Zr-pembrolizumab manufacturing according to GMP

To enable clinical application, GMP-compliant ^{89}Zr-pembrolizumab was developed. First, N-sucDf-pembrolizumab intermediate product was produced on a larger scale (60 mg batch, divided in 2.5 mg aliquots) and subsequently radiolabeled with ^{89}Zr, followed by purification, dilution and sterile filtration (online supplemental figure S1). Release specifications were defined, as shown in online supplemental table S1. All analytical methods for quality control (QC) were validated. According to protocol validation of both N-sucDf-pembrolizumab and ^{89}Zr-pembrolizumab, manufacturing consisted of three independent validation runs, including complete release QC. Stability of N-sucDf-pembrolizumab stored at −80 °C was studied up to 6 months and stability of ^{89}Zr-pembrolizumab was determined up to 168 hours at 2°C to 8°C stored in a sterile, type 1 glass injection vial. In addition, in use stability was demonstrated at RT in a polypropylene syringe for up to 4 hours (online supplemental table S2).

Statistical analysis

Data are presented as median±IQR. A Mann-Whitney U test, followed by a Bonferroni correction was performed to compare groups (GraphPad, Prism 7). P values ≤0.05 were considered significant. If not indicated otherwise, results were not statistically significant.

RESULTS

^{89}Zr-pembrolizumab development for in vivo studies

We optimized the conjugation processes of pembrolizumab with the TFP-N-sucDf chelator and its subsequent radiolabeling with ^{89}Zr. For in vivo studies, N-sucDf-pembrolizumab was produced with >60% yield and average 1.7 chelators per antibody (online supplemental figure S2, table S1). N-sucDf-pembrolizumab was subsequently radiolabeled with ^{89}Zr at a specific activity of 250 MBq/mg, with radiochemical purity of >95% after purification. Both N-sucDf-pembrolizumab and ^{89}Zr-pembrolizumab

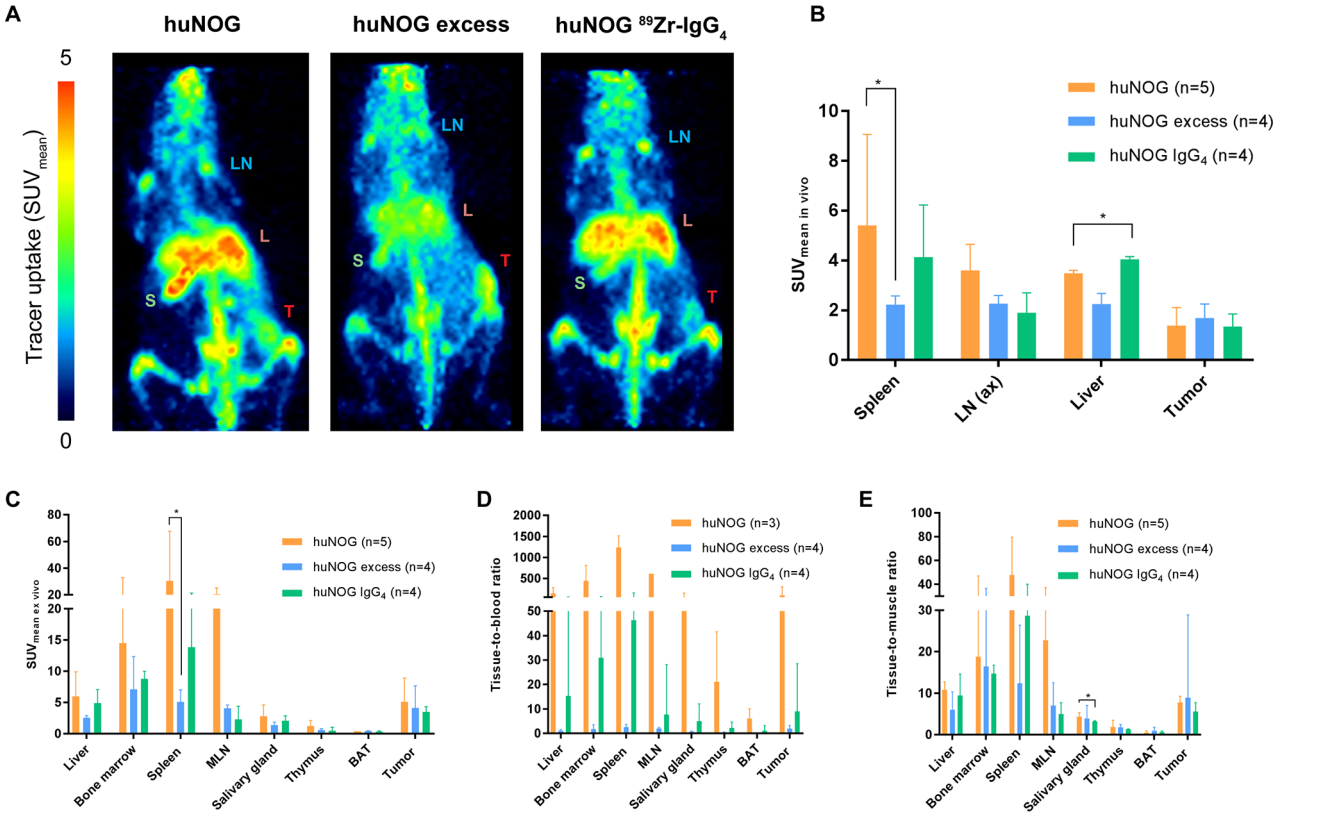

Figure 1 In vivo PET imaging and ex vivo biodistribution of ^{89}Zr-pembrolizumab in immunocompetent humanized NOG mice. Mice were xenografted with A375M tumor cells and received tracer injection at day 0. For blocking studies huNOG mice received a 10-fold excess of unlabeled pembrolizumab (huNOG excess). As a control for non-specific uptake huNOG mice were injected with ^{89}Zr-IgG$_4$. PET imaging performed on day 7 post injection (pi). (A) In vivo PET examples (maximum intensity projections) at day 7 pi showing uptake in tumor (T), axillary lymph nodes (LN), liver (L) and spleen (S). (B) In vivo uptake of ^{89}Zr-pembrolizumab in spleen, lymph nodes (axillary), liver and tumor, at day 7 pi. Uptake is expressed as SUV$_{mean}$. (C) Ex vivo biodistribution of ^{89}Zr-pembrolizumab in humanized NOG mice. Uptake is expressed as mean radioactivity per gram tissue, adjusted for total body weight (SUV$_{mean\ ex\ vivo}$). Data expressed as median±IQR *p≤0.05. BAT, brown adipose tissue; huNOG, humanized NOG mice; MLN, mesenteric lymph nodes; PET, positron emission tomography.

were stable, as shown in online supplemental table S1, S2 and figure S2. Immunoreactivity was not impaired by conjugation or radiolabeling.

^{89}Zr-pembrolizumab imaging and biodistribution in humanized mice

PET imaging revealed ^{89}Zr-pembrolizumab uptake in tumor, but also in healthy tissues, including liver, spleen and lymph nodes, of A375M tumor-bearing huNOG mice (figure 1A,B). Consistent with these results, ex vivo biodistribution at day 7 pi showed highest ^{89}Zr-pembrolizumab uptake in spleen (SUV$_{mean}$ 30.5, IQR 15.8 to 67.7), mesenteric lymph nodes (SUV$_{mean}$ 20.4, IQR 8.0 to 25.2), bone marrow (SUV$_{mean}$ 14.5, IQR 6.1 to 32.8), thymus (SUV$_{mean}$ 1.3, IQR 1.1 to 2.1), liver (SUV$_{mean}$, IQR 6.0, IQR 3.4 to 9.9) and tumor (SUV$_{mean}$ 5.1, IQR 3.3 to 8.9) (figure 1C, online supplemental table S3).

Tumor uptake of ^{89}Zr-pembrolizumab was variable and slightly higher than tumor uptake observed for ^{89}Zr-IgG$_4$ control, however not significant due to small groups of mice (SUV$_{mean}$ 5.1, IQR 3.3 to 8.9 vs SUV$_{mean}$ 3.5, IQR 2.7 to 4.4) (figure 1C). This may be explained by low PD-1 expression found in all tumors by immunohistochemical (IHC) analysis (figure 2). ^{89}Zr-pembrolizumab tumor-to-blood ratio also did not differ from ^{89}Zr-IgG$_4$ control (figure 1D).

^{89}Zr-pembrolizumab in huNOG mice showed higher uptake in lymphoid tissues compared with ^{89}Zr-IgG$_4$ control: spleen (SUV$_{mean}$ 13.9, IQR 7.1 to 21.4, NS, p=0.254), mesenteric lymph nodes (SUV$_{mean}$ 2.3, IQR 1.4 to 4.4, NS, p=0.114), salivary gland (SUV$_{mean}$ 2.1, IQR 1.2 to 2.9, NS, p=0.635), bone marrow (SUV$_{mean}$ 8.8, IQR 7.6 to 10.0, NS, p=1.714) and thymus (SUV$_{mean}$ 0.5, IQR 0.4 to 1.1, p=0.1714), indicating that ^{89}Zr-pembrolizumab uptake in these tissues is, at least partly, PD-1-mediated. ^{89}Zr-pembrolizumab tissue-to-blood (T:B) and tissue-to-muscle (T:M) ratios in lymphoid organs confirmed high uptake in these tissues (figure 1D,E). Additionally, relatively high ^{89}Zr-IgG$_4$ uptake was found in spleen, bone marrow and liver compared with other organs, suggesting ^{89}Zr-pembrolizumab uptake in these tissues is also due to Fcγ receptor (FcγR)-binding of the antibody's Fc-tail. High ^{89}Zr-IgG$_4$ uptake was less evident in lymph nodes and thymus.

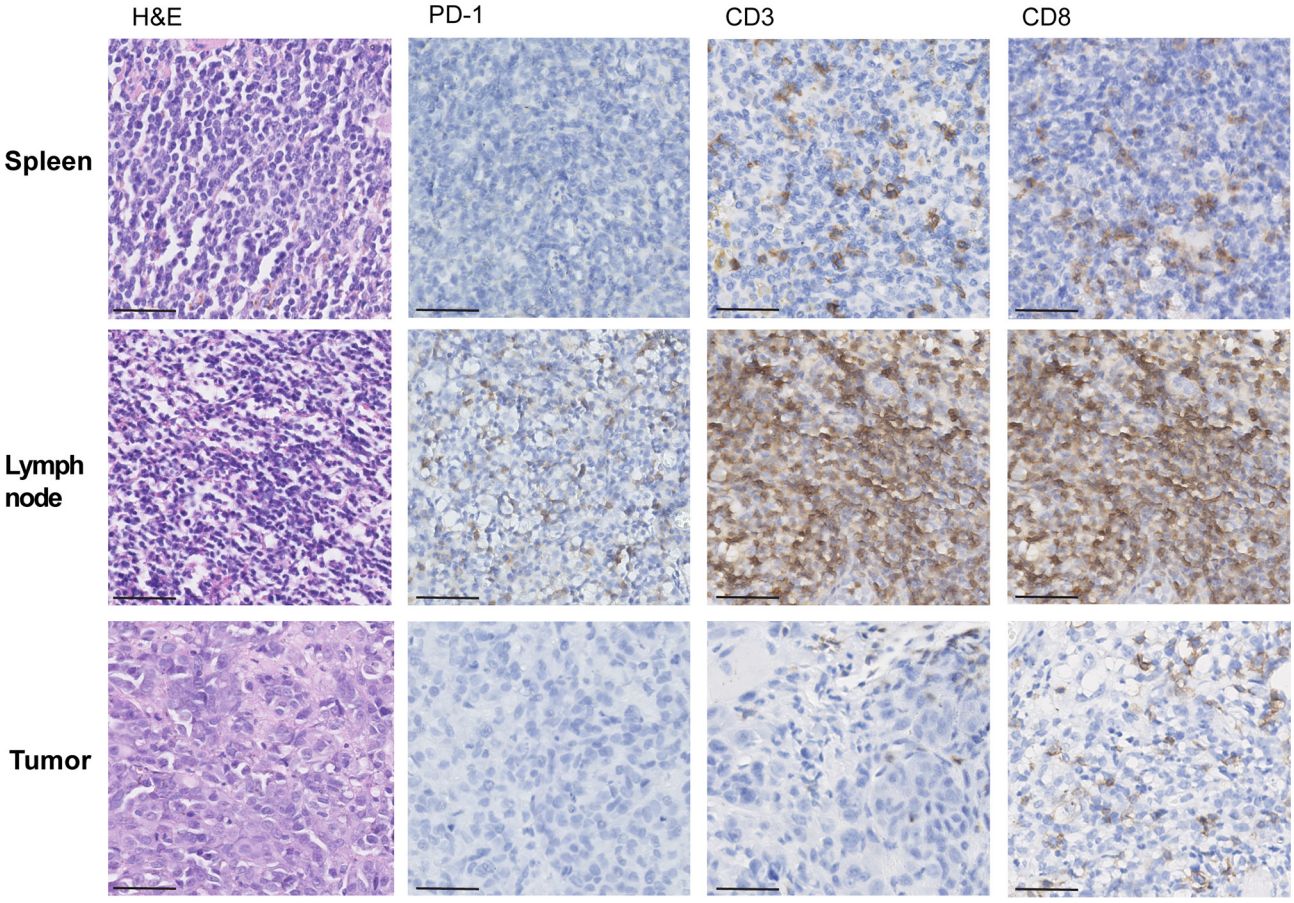

Figure 2 IHC analysis of spleen, mesenteric lymph node and tumor tissue humanized NOG mice. Formalin-fixed and paraffin embedded tissue blocks where cut into slices of 4 µM and stained for PD-1, CD3 and CD8 (40x). H&E staining served to analyze tissue viability and morphology (40x). Scalebar: 50 µm. IHC, immunohistochemical; PD-1, programmed cell death protein-1.

^{89}Zr-pembrolizumab spleen uptake in huNOG mice was blocked by the addition of a 10-fold excess unlabeled pembrolizumab (SUV_{mean} 30.5, IQR 15.8 to 67.7 versus SUV_{mean} 5.1, IQR 4.3 to 7.0, p=0.032) (figure 1B,C). Uptake in other lymphoid organs and liver was also reduced by addition of unlabeled mAb dose, whereas uptake in non-lymphoid tissues was unaffected (online supplemental table S3). Tracer activity in blood pool was increased by addition of unlabeled mAb (SUV_{mean} 0.1, IQR 0.0 to 1.8 to SUV_{mean} 2.2, IQR 1.4 to 7.4), but uptake in tumor did not change.

Autoradiography confirmed PET imaging results on a macroscopic level, showing high uptake in spleens of huNOG mice compared with spleens of mice that received an additional unlabeled pembrolizumab dose (figure 3). Furthermore, comparable tumor uptake was found for different dose groups. IHC analysis on spleen and lymph node tissue of huNOG mice revealed that PD-1, CD3 and CD8 positive cells were present. CD3 and CD8 cells were also present in tumor tissue of huNOG mice (figure 2), however, PD-1 staining of these tumors was negative.

^{89}Zr-pembrolizumab biodistribution in NOG control mice clearly showed a different pattern than in huNOG mice, with high uptake in liver (SUV_{mean} 16.9, IQR 5.1 to 26.2) and spleen (SUV_{mean} 49.6, IQR 16.6 to 135.6), whereas ^{89}Zr-pembrolizumab tumor uptake in NOG mice was similar to huNOG mice (SUV_{mean} 9.3, IQR 4.5 to 15.7 vs SUV_{mean} 5.1, IQR 3.3 to 8.9) (online supplemental figure S3). High ^{89}Zr-pembrolizumab spleen uptake in this model may be unexpected, since limited T-cells are present in NOG mice (online supplemental figure

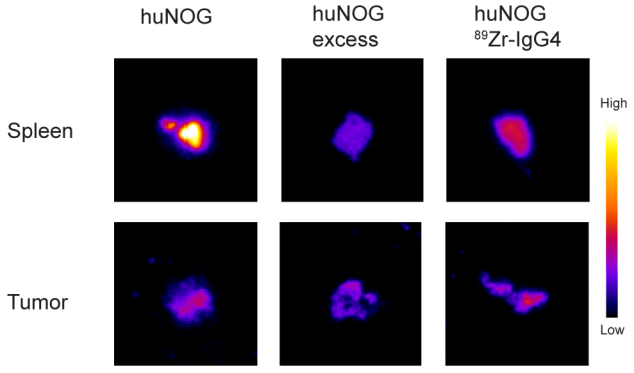

Figure 3 Autoradiography of spleen and tumor tissue humanized NOG mice (huNOG). Formalin-fixed and paraffin embedded tissue blocks where cut into slices of 4 µM. These slices were exposed to a phosphor imaging screen for 72 hours and were then scanned using a Cyclone phosphor imager.

S3). However, high spleen uptake in severely immunocompromised mice has been described previously and is potentially Fcγ receptor-mediated.[23 24 32] Moreover, spleen weights in NOG mice were lower than in huNOG mice (NOG: 0.017 g±0.015 g; huNOG: 0.037 g±0.016 g, p=0.036), which resulted in higher tracer uptake expressed as %ID per gram spleen tissue for NOG mice. A low spleen weight may result from high radiosensitivity of NOG splenocytes, which can lead to toxicity.[33]

Critical steps in ^{89}Zr-pembrolizumab manufacturing

The production processes for N-sucDf-pembrolizumab intermediate product and ^{89}Zr-pembrolizumab for in vivo studies were modified to comply with GMP requirements. In the conjugation reaction, pH is increased from 4.5 to 8.5, performed in small titration steps, as described earlier by Verel *et al*.[30] During this pH transition, precipitation occurred at 6.5 to 7.0, which was re-dissolved at pH >7.5. No precipitation was observed when pH was changed abruptly, for example, by buffer exchange, to pH 8.5 during conjugation and to pH 4.5 for removal of Fe(III). This indicates potential instability of pembrolizumab at pH 6.5 to 7.0. Formation of aggregates may be explained by the fact that pembrolizumab is an IgG_4 type mAb, which forms non-classical disulfide bonds. In contrast, IgG_1 type antibodies can only form classical disulfide bonds. There are many other determinants of antibody stability besides disulfide bond formation, however, this phenomenon was not seen previously with the radiolabeling of IgG_1 type antibodies.[31 33 34]

Immunoreactivity was not affected when pembrolizumab showed precipitation during pH transition, demonstrated by comparable IRF for precipitated N-sucDf-pembrolizumab and for non-precipitated N-sucDf-pembrolizumab (online supplemental figure S4). However, it is unknown whether the pembrolizumab structure is modified by the formation of precipitates. Therefore, the method for pH transition by buffer exchange was incorporated in the conjugation protocol for pembrolizumab. Production of clinical grade ^{89}Zr-pembrolizumab was performed as previously described by Verel *et al*.[30]

^{89}Zr-pembrolizumab GMP validation

Three consecutive batches of conjugated and radiolabeled pembrolizumab were produced at clinical scale and complied with all release specifications (online supplemental tables S1 and S2), indicating that our process for manufacturing clinical grade ^{89}Zr-pembrolizumab is consistent and robust. ^{89}Zr-pembrolizumab was obtained with a specific activity of 37 MBq/mg and mean IRF of 1.35±0.6 (n=3). Stability studies revealed that N-sucDf-pembrolizumab remained compliant to release specifications up to 6 months storage at −80°C, therefore N-sucDf-pembrolizumab shelf-life was set at 6 months. Stability studies are ongoing and shelf-life may be extended if future time points remain within specifications. Data obtained during process development and validation were used to compile the investigational medicinal product dossier (IMPD), which includes all information regarding quality control, production and validation of ^{89}Zr-pembrolizumab. Based on this IMPD, ^{89}Zr-pembrolizumab has been approved by competent authorities for use in clinical studies.

DISCUSSION

This study reveals ^{89}Zr-pembrolizumab whole-body distribution in tumor-bearing huNOG mice established with a broad set of developed immune cells. Tumor uptake of ^{89}Zr-pembrolizumab was markedly lower than uptake in lymphoid tissues such as spleen, lymph nodes and bone marrow, but higher than uptake in other organs. Importantly, high uptake in lymphoid tissues could be reduced with a 10-fold excess of unlabeled pembrolizumab. This contrasts with ^{89}Zr-pembrolizumab tumor uptake, which was not reduced by the addition of unlabeled pembrolizumab.

Our study nicely shows the in vivo behavior of ^{89}Zr-pembrolizumab, which, apart from IgG pharmacokinetics determined by its molecular weight and Fc tail, is predominantly driven by its affinity for PD-1 (Kd:~30 pM). The PD-1 cell surface receptor is primarily expressed on activated T-cells and pro B-lymphocytes, which are abundantly present in our huNOG mouse model. Lymphocytes are highly concentrated in organs that are key players of the immune system: lymph nodes, spleen, thymus, bone marrow as well as tonsils, adenoid and Peyer's patches. From our PET imaging and ex vivo biodistribution data, we learned that ^{89}Zr-pembrolizumab distributed mainly to lymphoid organs, where PD-1 expressing immune cells are present.

^{89}Zr-pembrolizumab showed relatively low and variable tumor uptake, however, this uptake could be visualized with PET imaging 7 days pi and was higher than in non-lymphoid tissues. We hypothesized there may be PD-1-mediated ^{89}Zr-pembrolizumab tumor uptake, but we also found tumor uptake for ^{89}Zr-IgG_4, suggesting part of the ^{89}Zr-pembrolizumab tumor uptake is FcγR-mediated. In our mouse model, few PD-1 positive immune cells may have traveled to the tumor, thereby potentially limiting ^{89}Zr-pembrolizumab tumor uptake. Interestingly, the addition of unlabeled pembrolizumab did not influence tumor uptake. This is likely caused by substantial increase of ^{89}Zr-pembrolizumab in blood pool as a direct consequence of adding excess unlabeled pembrolizumab, warranting a continuous pembrolizumab supply to the tumor.

Ex vivo immunohistochemical analysis revealed CD3 and CD8 positive lymphocytes were present in tumor, but limited PD-1-expression was found. Immune checkpoint protein expression status in tumor-infiltrating lymphocytes is highly dynamic.[35 36] This so-called 'immune phenotype' depends on several factors, including tumor type, location and mutational burden. Our results indicate that, whereas PD-1 expression may demonstrate large

variation, ^{89}Zr-pembrolizumab PET imaging is able to capture PD-1 dynamics in both tumor and healthy tissues.

Compared with earlier preclinical studies with radiolabeled pembrolizumab in the hNSG model, we found higher ^{89}Zr-pembrolizumab uptake in spleen and other lymphoid tissues.[23 24] This likely reflects the presence of multiple hematopoietic cell lineages, including B-cells, T-cells, NK-cells, dendritic cells and monocytes, and thus higher PD-1 expression, in our huNOG model compared with the hNSG model. Molecular imaging studies with radiolabeled antibodies generally show distribution to the spleen. It also known that Fc/FcγR-mediated immunobiology of the experimental mouse model plays a key role in the in vivo biodistribution and tumor targeting.[33] In our mouse model, we also observed ^{89}Zr-IgG$_4$ uptake in lymphoid tissues, indicating ^{89}Zr-pembrolizumab uptake in these organs may have an FcγR-mediated component. For most radiolabeled antibodies without an immune target, spleen uptake in patients is ~5 %ID/kg.[37] This supports the idea that, independent of their target, antibodies often show distribution to the spleen. However, spleen uptake may be higher if PD-1 or PD-L1 is present.

Pembrolizumab has an IgG$_4$κ backbone with a stabilizing SER228PRO sequence alteration in the Fc-region to prevent the formation of half molecules. The IgG$_4$ backbone of pembrolizumab may slightly differ from the IgG$_4$ control molecule that we used for our experiments, however, FcγR-binding affinity and kinetics of pembrolizumab appears to be very similar to IgG$_4$.[38] We, therefore, consider the used IgG$_4$ control molecule to provide a useful indication of the extent of FcγR-mediated uptake. In this respect, FcγR-mediated uptake may be present in the spleen but potentially also in liver and tumor, since these tissues demonstrate relatively high uptake of ^{89}Zr-IgG$_4$.

PD-1 is predominantly expressed on activated T-cells while its ligand PD-L1 is expressed by a broader range of immune cells as well as tumor cells. It is therefore to be expected that biodistribution of antibody tracers targeting PD-L1 may deviate from the biodistribution results that we described here for ^{89}Zr-pembrolizumab. In table 1, we presented an overview of preclinical imaging and biodistribution studies using anti-PD-1 and anti-PD-L1 tracers. Data turned out to be highly variable, mostly focused on tumor and not on the immune system, and therefore not just comparable. From our results, we increasingly realize that it is extremely important for interpretation of these type of data to know the characteristics of the antibody (origin, cross-reactivity, Fc-backbone, target, target-affinity and dose), the animal model (mouse strain, age, immune status and tumor cell line) and time points, variables we detailed in the table.

As for preclinical studies, data on the distribution of PD-1 and PD-L1 targeting antibodies to lymphoid organs in patients is still limited. A clinical imaging study in 13 patients demonstrated modest ^{89}Zr-nivolumab spleen uptake of SUV$_{mean}$ 5.8±0.7, whereas uptake of this radiolabeled antibody targeting PD-1 in other lymphoid tissues was not addressed.[39] ^{89}Zr-atezolizumab (anti-PD-L1 antibody) imaging in 22 patients revealed spleen uptake with an SUV$_{mean}$ of 15. ^{89}Zr-atezolizumab also distributed to other lymphoid tissues and sites of inflammation, whereas uptake in non-lymphoid organs was low. The high spleen uptake could at least partly be explained by presence of PD-L1 in endothelial littoral cells of the spleen.[40] To perceive what can be expected for ^{89}Zr-pembrolizumab PET imaging in patients, how results may be interpreted and potentially translated to predicting response, knowledge on which immune cells express PD-1 and where these cells are located in the human body is of utmost importance.

With our study, we validated the use of ^{89}Zr-pembrolizumab PET imaging to evaluate PD-1-mediated uptake in tumor and immune tissues in a setting that allowed for comparing tracer uptake and whole tumor tissue analysis. To enable evaluation of ^{89}Zr-pembrolizumab biodistribution in humans, we developed clinical grade ^{89}Zr-pembrolizumab. Clinical ^{89}Zr-pembrolizumab PET imaging in patients with melanoma and NSCLC before treatment with pembrolizumab is currently performed at our center (ClinicalTrials.gov Identifier NCT02760225), and may elucidate if tracer tumor uptake correlates to response and if uptake in healthy PD-1 expressing tissues correlates to toxicity.

CONCLUSION

We demonstrated the in vivo biodistribution of ^{89}Zr-pembrolizumab in humanized mice, and found uptake in tumor with the highest uptake in the lymphoid system, reflecting the presence of PD-1. Insight in the in vivo behavior and biodistribution of immune checkpoint targeting monoclonal antibodies might aid in better understanding immune checkpoint inhibition therapy and could potentially help explaining variation in response as well as potential toxicity due to uptake in healthy (immune) tissues.

Twitter Elisabeth G E De Vries @VriesElisabeth

Contributors ELvdV was involved in project design and conceptualization, was involved in tracer development and GMP validation, wrote the IMPD, performed animal studies, performed ex vivo analyses, data analysis and wrote the manuscript; DG was involved in study conceptualization, data analysis, performed ex vivo analyses and wrote the manuscript; LPdJ was involved in tracer development and GMP validation, performed animal studies, performed ex vivo analyses and edited the manuscript; AJS was involved in GMP validation, wrote the IMPD and edited the manuscript; EGEdV was involved in project design and conceptualization, supervised the study and edited the manuscript; MNLdH was involved in project design and conceptualization, supervised the study and edited the manuscript. All authors read and approved the final manuscript.

Funding The research leading to these results received funding from the Innovative Medicines Initiatives 2 Joint Undertaking under grant agreement No 116106 (TRISTAN). This Joint Undertaking receives support from the European Union's Horizon 2020 research and innovation program and EFPIA.

Competing interests EGEdV reports grants from IMI TRISTAN (GA no.116106), during the conduct of the study; consulting and advisory role for NSABP, Daiichi Sankyo, Pfizer, Sanofi, Merck, Synthon Biopharmaceuticals; grants from Amgen, Genentech, Roche, Chugai Pharma, CytomX Therapeutics, Nordic Nanovector,

G1 Therapeutics, AstraZeneca, Radius Health, Bayer, all made available to the institution, outside the submitted work.

Patient consent for publication Not required.

Provenance and peer review Not commissioned; externally peer reviewed.

Data availability statement Data are available upon reasonable request. The data sets used and/or analyzed during the current study are available from the corresponding author on reasonable request.

ORCID iDs
Elly L van der Veen http://orcid.org/0000-0001-6224-8114
Marjolijn N Lub-de Hooge http://orcid.org/0000-0002-5390-2791

REFERENCES

1 Postow MA, Sidlow R, Hellmann MD. Immune-Related adverse events associated with immune checkpoint blockade. *N Engl J Med* 2018;378:158–68.
2 Nguyen LT, Ohashi PS. Clinical blockade of PD1 and LAG3--potential mechanisms of action. *Nat Rev Immunol* 2015;15:45–56.
3 van der Veen EL, Bensch F, Glaudemans AWJM, *et al*. Molecular imaging to enlighten cancer immunotherapies and underlying involved processes. *Cancer Treat Rev* 2018;70:232–44.
4 Lamberts LE, Williams SP, Terwisscha van Scheltinga AGT, *et al*. Antibody positron emission tomography imaging in anticancer drug development. *J Clin Oncol* 2015;33:1491–504.
5 Heskamp S, Hobo W, Molkenboer-Kuenen JDM, *et al*. Noninvasive imaging of tumor PD-L1 expression using radiolabeled anti-PD-L1 antibodies. *Cancer Res* 2015;75:2928–36.
6 Josefsson A, Nedrow JR, Park S, *et al*. Imaging, biodistribution, and dosimetry of radionuclide-labeled PD-L1 antibody in an immunocompetent mouse model of breast cancer. *Cancer Res* 2016;76:472–9.
7 Chatterjee S, Lesniak WG, Gabrielson M, *et al*. A humanized antibody for imaging immune checkpoint ligand PD-L1 expression in tumors. *Oncotarget* 2016;7:10215–27.
8 Lesniak WG, Chatterjee S, Gabrielson M, *et al*. PD-L1 Detection in Tumors Using [^{64}Cu]Atezolizumab with PET. *Bioconjug Chem* 2016;27:2103–10.
9 Nedrow JR, Josefsson A, Park S, *et al*. Imaging of programmed cell death ligand 1: impact of protein concentration on distribution of anti-PD-L1 SPECT agents in an immunocompetent murine model of melanoma. *J Nucl Med* 2017;58:1560–6.
10 Kikuchi M, Clump DA, Srivastava RM, *et al*. Preclinical immunoPET/CT imaging using Zr-89-labeled anti-PD-L1 monoclonal antibody for assessing radiation-induced PD-L1 upregulation in head and neck cancer and melanoma. *Oncoimmunology* 2017;6:e1329071.
11 Truillet C, Oh HLJ, Yeo SP, *et al*. Imaging PD-L1 expression with ImmunoPET. *Bioconjug Chem* 2018;29:96–103.
12 Heskamp S, Wierstra PJ, Molkenboer-Kuenen JDM, *et al*. Pd-L1 microSPECT/CT imaging for longitudinal monitoring of PD-L1 expression in syngeneic and humanized mouse models for cancer. *Cancer Immunol Res* 2019;7:150–61.
13 Chatterjee S, Lesniak WG, Miller MS, *et al*. Rapid PD-L1 detection in tumors with PET using a highly specific peptide. *Biochem Biophys Res Commun* 2017;483:258–63.
14 Gonzalez Trotter DE, Meng X, McQuade P, *et al*. In vivo imaging of the programmed death ligand 1 by ^{18}F positron emission tomography. *J Nucl Med* 2017;25:1852–7.
15 Broos K, Keyaerts M, Lecocq Q, *et al*. Non-Invasive assessment of murine PD-L1 levels in syngeneic tumor models by nuclear imaging with nanobody tracers. *Oncotarget* 2017;8:41932–46.
16 Maute RL, Gordon SR, Mayer AT, *et al*. Engineering high-affinity PD-1 variants for optimized immunotherapy and immuno-PET imaging. *Proc Natl Acad Sci U S A* 2015;112:E6506–14.
17 Donnelly DJ, Smith RA, Morin P, *et al*. Synthesis and Biologic Evaluation of a Novel ^{18}F-Labeled Adnectin as a PET Radioligand for Imaging PD-L1 Expression. *J Nucl Med* 2018;59:529–35.
18 Mayer AT, Natarajan A, Gordon SR, *et al*. Practical immuno-PET radiotracer design considerations for human immune checkpoint imaging. *J Nucl Med* 2017;58:538–46.
19 Natarajan A, Patel CB, Ramakrishnan S, *et al*. A novel engineered small protein for positron emission tomography imaging of human programmed death ligand-1: validation in mouse models and human cancer tissues. *Clin Cancer Res* 2019;25:1774–85.
20 De Silva RA, Kumar D, Lisok A, *et al*. Peptide-Based ^{68}Ga-PET Radiotracer for Imaging PD-L1 Expression in Cancer. *Mol Pharm* 2018;15:3946–52.
21 Kumar D, Lisok A, Dahmane E, *et al*. Peptide-Based PET quantifies target engagement of PD-L1 therapeutics. *J Clin Invest* 2019;129:616–30.
22 Natarajan A, Mayer AT, Xu L, *et al*. Novel radiotracer for immunoPET imaging of PD-1 checkpoint expression on tumor infiltrating lymphocytes. *Bioconjug Chem* 2015;26:2062–9.
23 Natarajan A, Mayer AT, Reeves RE, *et al*. Development of novel immunoPET tracers to image human PD-1 checkpoint expression on tumor-infiltrating lymphocytes in a humanized mouse model. *Mol Imaging Biol* 2017;19:903–14.
24 England CG, Ehlerding EB, Hernandez R, *et al*. Preclinical pharmacokinetics and biodistribution studies of ^{89}Zr-labeled pembrolizumab. *J Nucl Med* 2017;58:162–8.
25 England CG, Jiang D, Ehlerding EB, *et al*. ^{89}Zr-labeled nivolumab for imaging of T-cell infiltration in a humanized murine model of lung cancer. *Eur J Nucl Med Mol Imaging* 2018;45:110–20.
26 Cole EL, Kim J, Donnelly DJ, *et al*. Radiosynthesis and preclinical PET evaluation of ^{89}Zr-nivolumab (BMS-936558) in healthy non-human primates. *Bioorg Med Chem* 2017;25:5407–14.
27 Natarajan A, Patel CB, Habte F, *et al*. Dosimetry Prediction for Clinical Translation of ^{64}Cu-Pembrolizumab ImmunoPET Targeting Human PD-1 Expression. *Sci Rep* 2018;8:633.
28 Hettich M, Braun F, Bartholomä MD, *et al*. High-Resolution PET imaging with therapeutic antibody-based PD-1/PD-L1 checkpoint tracers. *Theranostics* 2016;6:1629–40.
29 De La Rochere P, Guil-Luna S, Decaudin D, *et al*. Humanized mice for the study of immuno-oncology. *Trends Immunol* 2018;39:748–63.
30 Verel I, Visser GWM, Boellaard R, *et al*. 89Zr immuno-PET: comprehensive procedures for the production of 89Zr-labeled monoclonal antibodies. *J Nucl Med* 2003;44:1271–81.
31 Nagengast WB, de Vries EG, Hospers GA, *et al*. In vivo VEGF imaging with radiolabeled bevacizumab in a human ovarian tumor xenograft. *J Nucl Med* 2007;48:1313–9.
32 Liu H, May K. Disulfide bond structures of IgG molecules: structural variations, chemical modifications and possible impacts to stability and biological function. *MAbs* 2012;4:17–23.
33 Sharma SK, Chow A, Monette S, *et al*. Fc-Mediated anomalous biodistribution of therapeutic antibodies in immunodeficient mouse models. *Cancer Res* 2018;78:1820–32.
34 Dijkers ECF, Kosterink JGW, Rademaker AP, *et al*. Development and characterization of clinical-grade 89Zr-trastuzumab for HER2/neu immunoPET imaging. *J Nucl Med* 2009;50:974–81.
35 Havel JJ, Chowell D, Chan TA. The evolving landscape of biomarkers for checkpoint inhibitor immunotherapy. *Nat Rev Cancer* 2019;19:133–50.
36 Simon S, Labarriere N. Pd-1 expression on tumor-specific T cells: friend or foe for immunotherapy? *Oncoimmunology* 2017;7:e1364828.
37 Bensch F, Smeenk MM, van Es SC, *et al*. Comparative biodistribution analysis across four different ^{89}Zr-monoclonal antibody tracers-The first step towards an imaging warehouse. *Theranostics* 2018;8:4295–304.
38 Zhang T, Song X, Xu L, *et al*. The binding of an anti-PD-1 antibody to FcγRI has a profound impact on its biological functions. *Cancer Immunol Immunother* 2018;67:1079–90.
39 Niemeijer AN, Leung D, Huisman MC, *et al*. Whole body PD-1 and PD-L1 positron emission tomography in patients with non-small-cell lung cancer. *Nat Commun* 2018;9:4664.
40 Bensch F, van der Veen EL, Lub-de Hooge MN, *et al*. ^{89}Zr-atezolizumab imaging as a non-invasive approach to assess clinical response to PD-L1 blockade in cancer. *Nat Med* 2018;24:1852–8.